Pergamon

Geochimica et Cosmochimica Acta, Vol. 68, No. 12, pp. 2623–2637, 2004

0016-7037/04 $30.00 + .00

doi:10.1016/j.gca.2003.11.030

Copper(II) sorption onto goethite, hematite and lepidocrocite: A surface complexation model based on ab initio molecular geometries and EXAFS spectroscopy

CAROLINE L. PEACOCK and DAVID M. SHERMAN*
Department of Earth Sciences, University of Bristol, Bristol, BS8 1RJ, United Kingdom

(*Received August* 18, 2003; *accepted in revised form November* 10, 2003)

Abstract—We measured the adsorption of Cu(II) onto goethite (α-FeOOH), hematite (α-Fe_2O_3) and lepidocrocite (γ-FeOOH) from pH 2–7. EXAFS spectra show that Cu(II) adsorbs as $(CuO_4H_n)^{n-6}$ and binuclear $(Cu_2O_6H_n)^{n-8}$ complexes. These form inner-sphere complexes with the iron (hydr)oxide surfaces by corner-sharing with two or three edge-sharing $Fe(O,OH)_6$ polyhedra. Our interpretation of the EXAFS data is supported by ab initio (density functional theory) geometries of analogue $Fe_2(OH)_2(H_2O)_8Cu(OH)_4$and $Fe_3(OH)_4(H_2O)_{10}Cu_2(OH)_6$ clusters. We find no evidence for surface complexes resulting from either monodentate corner-sharing or bidentate edge-sharing between $(CuO_4H_n)^{n-6}$ and $Fe(O,OH)_6$ polyhedra. Sorption isotherms and EXAFS spectra show that surface precipitates have not formed even though we are supersaturated with respect to CuO and $Cu(OH)_2$. Having identified the bidentate $(\equiv FeOH)_2Cu(OH)_2^0$ and tridentate $(\equiv Fe_3O(OH)_2)Cu_2(OH)_3^0$ surface complexes, we are able to fit the experimental copper(II) adsorption data to the reactions

$$3(\equiv FeOH) + 2Cu^{2+} + 3H_2O = (\equiv Fe_3O(OH)_2)Cu_2(OH)_3^0 + 4H^+$$

and

$$2(\equiv FeOH) + Cu^{2+} + 2H_2O = (\equiv FeOH)_2Cu(OH)_2^0 + 2H^+.$$

The two stability constants are similar for the three iron (hydr)oxide phases investigated. *Copyright © 2004 Elsevier Ltd*

1. INTRODUCTION

The aqueous geochemistry of copper can be strongly controlled by sorption onto iron and manganese (hydr)oxides and clay minerals. In soils, copper is concentrated into the clay fraction (Le Riche and Weir, 1963) presumably by sorption onto colloidal FeOOH phases. In lacustrine sediments, there is clear evidence of the copper-FeOOH association: Tessier et al. (1985) showed that Cu was bound to Mn- and Fe-oxides and that the pore waters were undersaturated with respect to all Cu solid phases. Adsorption of copper to FeOOH phases controls the release of copper during sulfide oxidation (Bonnissel-Gissinger et al., 1998; Juang and Wu, 2002; Öhlander et al., 2003).

In the deep oceans, the Cu-FeOOH association is less clear: in the lower water column, copper is scavenged by the particulate fraction (Boyle et al., 1977) but released during early diagenesis at the ocean floor (e.g., Vanos et al., 1993). The resulting benthic source enriches bottom waters in copper (Boyle et al., 1977); however, if Fe-Mn oxide hydroxide phases are forming at the sediment-water interface, the flux of Cu into bottom water is diminished (Callender and Bowser, 1980; Fernex, 1992). Adsorption of Cu(II) onto colloidal iron oxides produced at hydrothermal vents at mid ocean ridges does occur (Feely, 1992; Bogdanov, 1997; Savenko, 2001) but is not a major control on the concentration of copper in seawater (Elderfield and Schultz, 1996). The incorporation of Cu in metal-rich ridge-crest sediments is a minor component of the overall cycle of the element in the deep water column (Boyle et al., 1977).

Iron oxyhydroxide phases commonly form as reactive, high-surface area secondary minerals resulting from surface weathering processes. Goethite (α-FeOOH) is ubiquitous in natural systems, occurring in virtually all weathering environments, whilst hematite (α-Fe_2O_3) is widespread in the soils of tropical and subtropical regions (Schwertmann and Cornell, 1991). Lepidocrocite (γ-FeOOH) occurs as a major iron oxyhydroxide under acid mine drainage (AMD) conditions (Herbert, 1995) and commonly forms via oxidation of Fe^{2+} phases such as green rust (a mixed Fe^{2+}/Fe^{3+} oxyhydroxide; Schwertmann and Fechter, 1994) and amorphous FeS (s) (Fendorf et al., 1997).

Previous studies examining the interaction between Cu(II) and iron oxyhydroxide minerals have tended to focus on either the modeling of adsorption behavior displayed in experimental adsorption edges and isotherms, or direct spectroscopic investigation of the metal-mineral association.

Two types of modeling approach have been followed: surface complexation modeling (SCM) and a more empirical consideration involving the use of Langmuir or similar equations to describe adsorption data (Angove et al., 1999). Both SCM and empirical modeling frameworks have successfully described the adsorption of Cu(II) to goethite and hematite by invoking $\equiv SOCu^+$ surface complexes (e.g., Jung et al., 1998; Christl and Kretzschmar, 1999; Buerge-Weirich, 2002), ≡SOCuOH surface complexes (Rodda et al., 1996), or a combination of both $\equiv SOCu^+$ and ≡SOCuOH surface complexes (Robertson and Leckie, 1998). Using the competitive Langmuir model, Rodda et al. (1996) successfully described Cu(II) ad-

* Author to whom correspondence should be addressed (dave.sherman@bristol.ac.uk).

sorption to goethite through the competitive adsorption of monomeric $CuOH^+$ and dimeric $Cu_2(OH)_2^{2+}$, the dimer adsorbing more strongly to the mineral surface. Katz and Hayes (1995a,b) drew on spectroscopic evidence and recommend the use of polymer species within the SCM framework to adequately describe adsorption at higher surface loadings. Modeling Cu(II) adsorption onto iron (hydr)oxide phases in the presence of natural organic matter (NOM) has also received much attention (e.g., Nowack et al., 1996; Christl and Kretzschmar, 2001; Buerge-Weirich et al., 2002) as oxide mineral surfaces in many natural environments can be coated with adsorbed NOM (Davis, 1982; O'Melia, 1989).

Direct spectroscopic investigations of Cu(II)-iron oxyhydroxide adsorption revealed inner-sphere surface complexes (e.g., Bochatay et al., 1997) consistent with modeling results. Several studies also reported the presence of small multinuclear clusters bound by inner-sphere complexation at the iron oxyhydroxide surface. Bochatay et al. (1997) attributed a second shell of metal atoms at 2.96 Å to Cu atoms associated with hydroxo-bridged Cu^{2+} surface polymers, while Parkman et al. (1999) reported Cu-Cu/Fe-Cu at 2.92 Å on goethite and Cu-Cu/Fe-Cu at 3.04 Å on lepidocrocite. Farquhar et al. (1997) also reported Cu-Cu interactions at 2.65 Å (average) and 3.11 Å on muscovite and biotite respectively.

To date, however, no study has attempted to develop a surface complexation model of Cu sorption constrained by results from spectroscopy. Here, we fit sorption edges and isotherms to a surface complexation model based on surface species determined from EXAFS spectroscopy. The interpretation of EXAFS spectra is aided using first-principles (density functional theory) calculations of surface complex geometries. Since the surface complexation model will be based on the actual surface species, we believe our results will be more reliable when applied to modeling reactive transport of Cu in complex natural systems.

2. EXPERIMENTAL METHODS

2.1. Mineral Preparation and Characterization

Goethite, hematite and lepidocrocite were synthesized from AR grade reagents using the methods of Schwertmann and Cornell (1991). Goethite was prepared by hydrolysis of a $Fe(NO_3)_3$ solution at pH 12–13 and 70°C for 60 h. Hematite was prepared by hydrolysis of a $Fe(NO_3)_3$ solution held at 98°C for 7 d. Lepidocrocite was prepared by the oxidation/hydrolysis of a $FeCl_2$ solution at pH 6.7–6.9. Plastic labware was used throughout. Mineral identity and purity was confirmed by X-ray powder diffraction (XRD) analysis of randomly orientated powder samples. The surface areas of the synthesized goethite, hematite and lepidocrocite were measured by BET to be 32.73 ± 3 m^2/g, 30.02 ± 3 m^2/g and 75.24 ± 3 m^2/g respectively.

2.2. Potentiometric Titration

Goethite, hematite and lepidocrocite potentiometric titrations were carried out at three salt concentrations (0.003 mol/L, 0.01 mol/L and 0.1 mol/L $NaNO_3$) following the method of Hayes et al. (1991). The dried solid mineral was suspended in preboiled, nitrogen-purged (<1 ppm CO_2 (g)) 18.2 mΩ Milli-Q water and nitrogen-purged (<1 ppm CO_2 (g)) overnight before titrations. Initial pH of the goethite, hematite and lepidocrocite solutions after overnight purging were approximately pH 8, 8.5 and 7.2 respectively. Titrations were performed at 25°C in an air-tight reactor with constant stirring to prevent settling. Base (NaOH, free from carbonate), acid (HNO_3) and salt solutions ($NaNO_3$) were prepared from stock solutions and added via an automated titrator. A nitrogen atmosphere (<1 ppm CO_2 (g)) was maintained throughout the experiment. Electrolyte was added to adjust the ionic strength to 0.003 mol/L and acid then added to gradually lower the pH to approximately pH 4 (see Hayes et al., 1991). Incremental addition of base then produced a titration from approximately pH 4 −11. After each incremental addition of base, 5 min were allowed for pH equilibration. The suspension was returned to pH ~4 by reverse acid titration, electrolyte added to adjust the ionic strength to the next level and the titration repeated following the same method. Goethite, hematite and lepidocrocite concentration in solution were 6.63 and 5 g/L respectively. In agreement with other titration studies (e.g., Hayes et al., 1991; Robertson and Leckie, 1998; Venema et al., 1998) we observed no significant hysteresis between the acid and base titration legs.

We used a pin-tip double junction glass combination electrode (Sentek) with a salt bridge of 3 mol/L $NaNO_3$. The electrode was calibrated potentiometrically following the method of Gans (2000).

The base leg of the titrations are reported here and used to optimize acid-base parameters for use in mineral-copper surface complexation modeling.

2.3. Sample Synthesis

Goethite, hematite and lepidocrocite batch experiments were prepared with copper II aqueous solution using AR grade reagents and 18.2 mΩ Milli-Q water. All solutions and resulting experimental suspensions were purged with Ar (g) or N_2 (g) (<1 ppm CO_2 (g)) and all adsorption experiments were conducted at 25°C. pH measurements were calibrated to ± 0.05 pH units using Whatman NBS grade buffers.

2.3.1. pH Adsorption Edge Experiments

Copper II stock solution was prepared at 100 ppm from $Cu(NO_3)_2.3H_2O$. Adsorption pH experiments at 25 ppm $[Cu]_{total}$ were prepared by adding 7.5 mL of 100 ppm Cu stock solution to 0.1 g sorbent (goethite, hematite or lepidocrocite) in 22.5 mL of 0.1 mol/L $NaNO_3$. Sorbent concentration in solution was therefore 3.33 g/L. The resulting suspensions were immediately shaken and initial pH was recorded after stabilization to two decimal places. Suspension pH was then varied from pH 2 −7 by the dropwise addition (<1 mL) of HNO_3/NaOH and recorded after stabilization to two decimal places. Adsorption pH experiments were then shaken continuously for 4 weeks. Adsorption of Cu to goethite at 25 ppm $[Cu]_{total}$ was investigated with EXAFS spectroscopy of specific samples from the adsorption edge at pH ~4.7 and 6.3. Goethite samples at pH ~4.7 and 6.3 contained 0.38 and 0.75 wt% copper with estimated surface coverage (calculated assuming 6 sites/nm^2 and 32.73 m^2/g) at 17.8% and 34.9% respectively. Adsorption of Cu to hematite at 25 ppm $[Cu]_{total}$ was investigated with EXAFS spectroscopy of a specific sample from the adsorption edge at pH ~5.3, containing 0.73 wt% copper with estimated surface coverage (calculated assuming 7.5 sites/nm^2 and 30.02 m^2/g) at 46%. Adsorption of Cu to lepidocrocite at 25 ppm $[Cu]_{total}$ was investigated with EXAFS spectroscopy of specific samples from the adsorption edge at pH ~4.6, 5 and 6.4. Lepidocrocite samples at pH ~4.6, 5 and 6.4 contained 0.2, 0.43 and 0.75 wt% Cu with estimated surface coverage (calculated assuming 1.6 sites/nm^2 and 75.24 m^2/g) at 13.8%, 30.4% and 52.3% respectively.

2.3.2. Constant-pH Isotherm Experiments

Goethite, hematite and lepidocrocite constant pH experiments were prepared by adding 3–15 mL of 100 ppm Cu stock solution to 0.1 g sorbent (goethite, hematite or lepidocrocite) in 27–15 mL of 0.1 mol/L $NaNO_3$ respectively. Sorbent concentration in solution was therefore 3.33 g/L, and $[Cu]_{total}$ ranged from 10–50 ppm. The resulting suspensions were immediately shaken and initial pH was recorded after stabilization to two decimal places. Suspension pH was then set at pH 6.5 by the dropwise addition (<1 mL) of NaOH and recorded after stabilization to two decimal places. Plastic centrifuge tubes containing the suspensions were then shaken continuously for 4 weeks.

Batch adsorption samples were separated by centrifugation (10,000 rpm for 10–15 min) into an adsorption sample (thick paste) for spectroscopic analysis and a clear supernate for determination of total copper concentration. Supernates were filtered using 0.2 μm cellulose

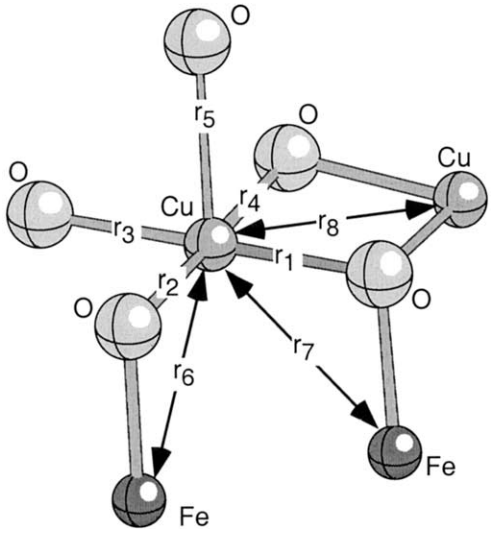

Fig. 1. Multiple scattering configuration used in EXAFS fits for Cu(II) sorbed to goethite, hematite and lepidocrocite.

nitrate membrane filters, acidified with 1% HNO_3 and analyzed for copper by inductively-coupled plasma atomic emission spectrometry (ICP-AES). All adsorption samples were spectroscopically analyzed either immediately after centrifugation or after storage at 1–4°C for a maximum of 48 h.

2.4. EXAFS Data Collection and Analysis

2.4.1. Data Collection

EXAFS fluorescence spectra of the copper K edge (8.979 keV) were collected on station 16.5 at the CLRC Synchrotron Radiation Source, Daresbury Laboratory, UK. Adsorption samples were presented to the X-ray beam as a wet paste held by Sellotape in a 2 mm-thick Teflon slide with a 4 × 15 mm sample slot. During data collection, storage ring energy was 2.0 GeV and the beam current varied between 130 and 240 mA. The monochromator was set to reject 50% of the incoming beam to minimize higher harmonics in the EXAFS spectrum. EXAFS data were collated from up to 10 fluorescence mode scans using an Ortec 18-element solid state detector.

It should be noted that EXAFS cannot discriminate between Cu and Fe using phase and amplitude functions alone. Next-nearest neighbor distances in section 3.1 are therefore Fe or Cu.

2.4.2. Data Analysis

EXAFS data reduction was performed using Daresbury Laboratory software (EXCALIB and EXBACK, Dent and Mosselmans, 1992). EXCALIB was used to calibrate from monochromator position (millidegrees) to energy (eV) and to average multiple spectra from individual samples. EXBACK was used to define the start of the EXAFS oscillations (determined from the inflection point on the K edge) and perform background subtraction. The preedge was fit to a linear function and the postedge background to two second-order polynomial segments. EXAFS were fit in the small atom approximation and we allowed for multiple scattering as coded in EXCURV98 (Binsted, 1998). The phase-shift functions used in the curve fitting were derived by ab initio methods in EXCURV98 using Hedin-Lundqvist potentials (Hedin and Lundqvist, 1969) and von Barth ground states. No Fourier filtering was performed during the data analysis.

The inclusion of multiple scattering improved the fit in the 3.5–4.5 Å region where some of the features result from O-O scattering within the square planer CuO_4^{6-} clusters. Multiple scattering calculations require specification of the full three dimensional structure of the Cu coordination environment (i.e., bond angles in addition to bond lengths). This was done using a hypothetical model cluster (Fig. 1) with C_1 symmetry. Note that the multiple-scattering contributions were calculated self-consistently during the EXAFS fits. Multiple scattering paths were limited to those involving 5 atoms although using only 3 atoms gave similar results. Multiple scattering path lengths were limited to 10 Å.

2.5. Density Functional Calculations

Quantum mechanical calculation of cluster geometries and energies were performed using the ADF 2.0 code (te Velde et al., 2001) which implements density functional theory for finite clusters and molecules using the linear combination of atomic orbital formalism. Molecular orbitals in the ADF code are constructed from Slater-type atomic orbitals, consisting of a Cartesian part $r^{kr}x^{kx}y^{ky}z^{kz}$ with $k_x + k_y + k_z = l$ (l = angular momentum quantum number) and an exponential part $e^{-\alpha r}$. Density functional theory allows a very large basis set to be used: For all atoms we used an uncontracted, triple-zeta basis set with polarization functions (i.e., 1s2s2p3s3p3d3d′3d″4s4s′4s″ + 4p for iron, 1s2s2s′2s″ + 3d for oxygen, 1s2s2p3s3p3d3d′3d″4s4s′4s″ + 4p for copper and 1s1s′1s″ + 2p for hydrogen). The charge density was also fit to a Slater-type orbital basis set. For all atoms except hydrogen, we used frozen core orbitals (i.e., 1s, 2s, 2p and 3p for Fe; 1s for O and 1s, 2s, 2p and 3p for Cu).

We used the Vosko et al. (1980) parameterization for the local exchange-correlation functionals together with generalized gradient corrections of Perdew et al. (1992). All calculations were performed using the spin-unrestricted formalism and we set the cluster to have a ferromagnetic configuration. The choice of ferromagnetic vs. antiferromagnetic configuration for the $Fe_2(OH)_2(H_2O)_8/Fe_3(OH)_4(H_2O)_{10}$ substrate should only have a minor chemical effect. (Note that a spin-restricted calculation would be seriously in error, however, since it would mix in configurations associated with high energy multiplets as discussed by Sherman, 1985.)

The geometries of the clusters were optimized using a Newton-Raphson method and Broydon-Fletcher update of the Hessian matrix as coded in ADF 2.0. During the geometry optimizations the total energies were converged to ± 5 kJ/mole.

2.6. Surface Complexation Modeling

The program FITEQL v3.2 (Herbelin and Westall, 1996) was used to fit the acid-base behavior of the mineral surfaces and subsequently the adsorption behavior of copper on goethite, hematite and lepidocrocite to a surface complexation model. The diffuse layer model (DLM, Dzombak and Morel, 1990) and triple layer model (TLM, Hayes and Leckie, 1987; Hayes et al., 1988) were used to account for surface electrostatics. FITEQL is used extensively for the calculation of chemical equilibrium constants in metal adsorption studies (e.g., Lovgren et al., 1990; Hayes et al., 1991; Jung et al., 1998; Robertson and Leckie, 1998; Ikhsan et al., 1999; Tadanier and Eick, 2002). The quality of the fits produced is given by:

$$V(Y) = (Y/S_Y)^2/(n_p{*}n_{II} - n_u) \quad (1)$$

where Y is the actual error in the mass balance equation, S_Y is the estimated experimental error given by FITEQL and the reciprocal of the variance S_Y is the weighting factor. n_p is the number of data points, n_{II} is the number of chemical components with known total and free concentrations, and n_u is the number of adjustable parameters (Lumsdon and Evans, 1994; Gao and Mucci, 2001). A good fit to experimental metal binding data is indicated by a value of V(Y) between 0.1 and 20 (Herbelin and Westall, 1996).

3. RESULTS AND DISCUSSION

3.1. Sorption of Cu^{2+} on Goethite, Hematite, and Lepidocrocite

3.1.1. Adsorption pH Edge Data

The aqueous speciation of Cu^{2+} at 25 ppm $[Cu]_{total}$ (calculated by suppressing the formation of CuO and $Cu(OH)_2$) is

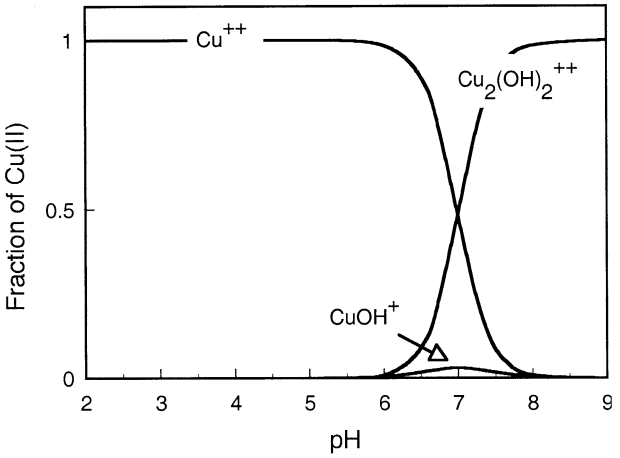

Fig. 2. Speciation of copper(II) as a function of pH. $[Cu]_{total} = 3.94 \times 10^{-4}$ molal (~25 ppm) in 0.1 mol/L $NaNO_3$. Calculated by suppressing the formation of CuO (s) and $Cu(OH)_2$ (s). Hydrolysis stability constants from Baes and Mesmer (1976).

shown in Figure 2 as a function of pH. Between pH ~2–6.5, Cu(II) occurs predominantly as the Cu^{2+} aqueous cation. Above pH ~7, the major hydrolysis product is $Cu_2(OH)_2^{2+}$. At 25 ppm $[Cu]_{total}$ and between pH ~2–6.5, Cu(II) therefore likely sorbs as Cu^{2+} (aq) and we find a sigmoid adsorption edge for goethite, hematite and lepidocrocite (Figs. 3, 4 and 5, respectively). The shape of our adsorption edges are in good agreement with several previous studies of Cu^{2+} adsorption onto iron oxyhydroxides (e.g., for goethite, Balistrieri and Murray, 1982; Ali and Dzombak, 1996; for hematite, Christl and Kretzschmar, 2001).

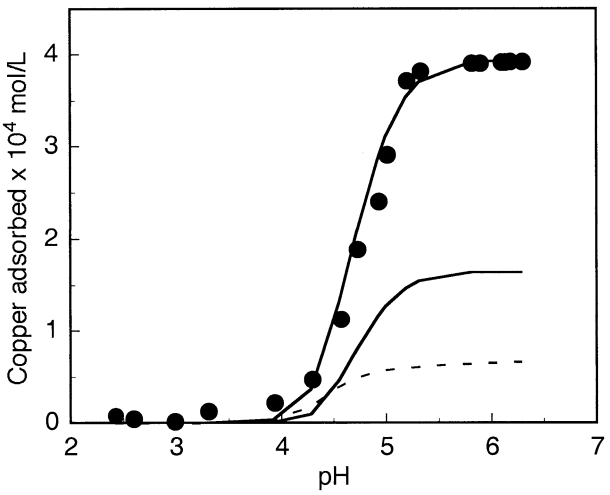

Fig. 4. Adsorption of copper(II) ions to hematite (α-Fe_2O_3, 3.33 g/L) as a function of pH at $I = 0.1$ mol/L $NaNO_3$ and 25°C, after 4 weeks equilibration time with 25 ppm $[Cu]_{total}$. Symbols are data points, lines are DLM fits showing total and individual surface species. Solid line = tridentate-dimer complex; dashed line = bidentate-mononuclear complex. Note that the concentration of copper due to the tridentate-dimer complex is twice that represented by the individual surface species solid line.

3.1.2. Constant pH Isotherm Data

Constant pH sorption data for goethite, hematite and lepidocrocite at pH 6.5 (Fig. 6) is plotted as final aqueous [Cu] (log) against the surface density of adsorbed ions, Γ (log mol/m^2). Saturation of CuO (s) and $Cu(OH)_2$ (s) is predicted to occur when log $[Cu^{2+}]$ mol/L is −5.8 (~0.1 ppm) and −4.8 to −4.5 (~1–2 ppm), respectively. However, at the nominal saturation

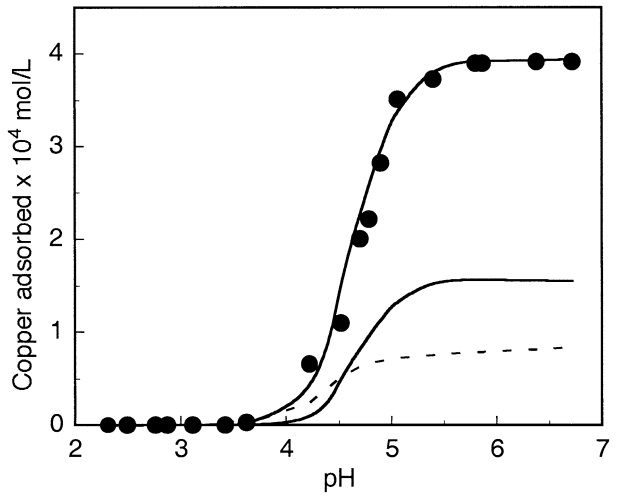

Fig. 3. Adsorption of copper(II) ions to goethite (α-FeOOH, 3.33 g/L) as a function of pH at $I = 0.1$ mol/L $NaNO_3$ and 25°C, after 4 weeks equilibration time with 25 ppm $[Cu]_{total}$. Symbols are data points, lines are DLM fits showing total and individual surface species. Solid line = tridentate-dimer complex; dashed line = bidentate-mononuclear complex. Note that the concentration of copper due to the tridentate-dimer complex is twice that represented by the individual surface species solid line.

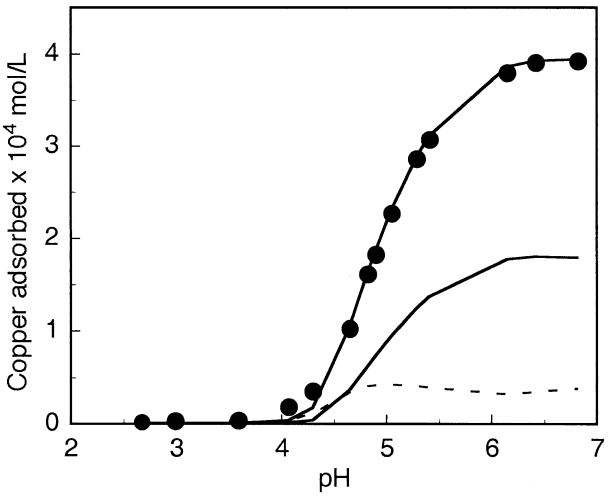

Fig. 5. Adsorption of copper(II) ions to lepidocrocite (γ-FeOOH, 3.33 g/L) as a function of pH at $I = 0.1$ mol/L $NaNO_3$ and 25°C, after 4 weeks equilibration time with 25 ppm $[Cu]_{total}$. Symbols are data points, lines are DLM fits showing total and individual surface species. Solid line = tridentate-dimer complex; dashed line = bidentate-mononuclear complex. Note that the concentration of copper due to the tridentate-dimer complex is twice that represented by the individual surface species solid line.

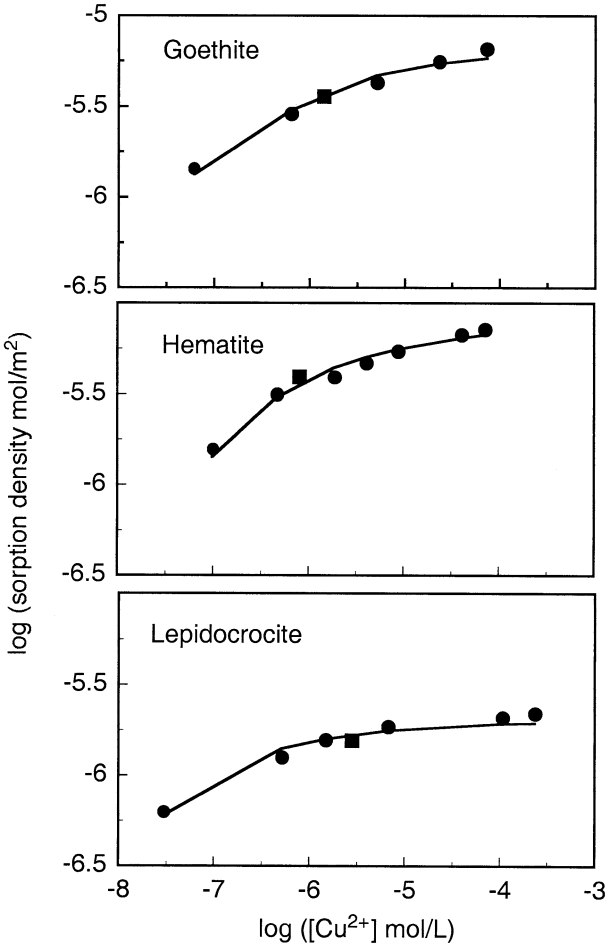

Fig. 6. Adsorption of copper(II) ions to goethite, hematite and lepidocrocite (3.33 g/L) at pH 6.5 (constant), I = 0.1 mol/L $NaNO_3$, and 25°C, after 4 weeks equilibration time with 10–50 ppm $[Cu]_{total}$. Symbols are data points; lines are DLM fits showing total surface species.

conditions, the surface density of "sorbed" ions does not increase sharply with $[Cu^{2+}]$ (Fig. 6). A sharp increase in $[Cu^{2+}]$ at log $[Cu^{2+}]$ mol/L ~−4.8 to −4.5 would be expected if precipitation of $Cu(OH)_2$ (s) was occurring. This is contrary to the results of Karthikeyan and Elliott (1999) and Karthikeyan et al. (1999) for Cu^{2+} adsorption on HFO where constant pH isotherm data (pH 6.9) clearly showed a sharp increase in the surface density of adsorbed ions at ~3.58 ppm $[Cu^{2+}]$. The absence of $Cu(OH)_2$ (s) precipitation in our experiments at [Cu] = 3.58 ppm presumably reflects the somewhat lower pH (6.5 vs. 6.9) at which we measured the isotherms.

Following Karthikeyan and Elliott (1999), we plot data points (square) on the goethite, hematite and lepidocrocite constant pH isotherms (Fig. 6) corresponding to the adsorption pH edge condition at pH ~6.5 represented in Figures 3, 4 and 5, respectively. These points lie in the region assigned as being dominated by adsorption (Karthikeyan and Elliott, 1999) and furthermore are well below the $[Cu^{2+}]$ required for the precipitation of $Cu(OH)_2$ (s).

Karthikeyan and Elliott (1999) and Karthikeyan et al. (1999) successfully modeled their constant pH isotherm and pH edge data with the surface precipitation model including the formation of $Cu(OH)_2$ (s). However, Karthikeyan and Elliott (1999) noted that interaction between Cu and HFO could be dominated by surface precipitation reactions or sorption of polymeric species. Katz and Hayes (1995a,b) also noted the need for multinuclear complexes to explain adsorption at moderate to high surface coverages.

As discussed below, EXAFS spectra are consistent with the absence of precipitation on the mineral surface, at least up to pH 6.5, in the constant pH isotherm (and pH edge) experiments. Our constant pH isotherm and pH edge data can, therefore, be used to develop a surface complexation model rather than a surface precipitation model as employed by Karthikeyan and Elliott (1999).

3.1.3. *Cu K-edge EXAFS Spectroscopy and Ab Initio Molecular Geometries*

Cu K-edge EXAFS (and Fourier transforms of the EXAFS) for wet-paste goethite hematite and lepidocrocite adsorption samples are shown in Figures 7, 8 and 9, respectively, and summarized in Table 1. Note, again, that we are fitting the spectra in terms of single-atom shells in a cluster with C_1 symmetry to allow for self-consistent inclusion of multiple scattering. At pH ~4, 5 and 6 we find the copper first-shell coordination environment to have 4.0 O at ~1.85–2.05 Å consistent with the protonated square-planar $(CuO_4H_n)^{n-6}$ ion. This is expected given the Jahn-Teller distortion of the d^9 Cu^{2+} ion. The range of Cu-O distances and small Debye-Waller factors of the O shells may be an artifact of fitting the four oxygens to four distinct shells. Attempts to constrain the Cu-O distances to be equal (but with larger Debye-Waller factors) gave less satisfactory fits. The ab initio geometries (discussed below) predict that the four shortest Cu-O bond lengths in the surface complexes range from 1.92 to 2.12 Å. Inclusion of an axial oxygen with a larger distance and Debye-Waller factor than the equatorial oxygens in the Cu coordination shell gives a slight improvement to the fits.

Beyond the oxygen shells, we find 1.0 next-nearest-neighbor atoms (Cu or Fe) at ~2.9 Å. We interpret the 2.9 Å distance to result from polymerization of $(CuO_4H_n)^{n-6}$ complexes to give $(Cu_2O_6H_n)^{n-8}$ dimers. We find an additional next-nearest-neighbor shell corresponding to 2 Fe atoms at a distance of 3.2–3.4 Å. Note that we constrained the Debye-Waller factors to be constant for the 2.9 and 3.2–3.4 Å shells. We interpret these distances as resulting from bidentate corner-sharing between $(CuO_4H_n)^{n-6}$ complexes and edge-sharing $Fe(O,OH)_6$ polyhedra (Fig. 10a) or by tridentate corner-sharing between $(Cu_2O_6H_n)^{n-8}$ dimers and three edge-sharing $Fe(O,OH)_6$ polyhedra (Fig. 10b).

The features in the Fourier transform of the EXAFS at distances greater than 3.5 Å appear to result from multiple scattering. We are able to model the first peak (near 3.9 Å) fairly well using paths including only 3 atoms. The peaks at greater distances (>4.0 Å) cannot be very accurately modeled in terms of multiple scattering within the small cluster used here (Fig. 1). Some of this structure is also due to noise. Surface complexes resulting from monodentate corner-sharing between $(CuO_4H_n)^{n-6}$ and $Fe(O,OH)_6$ polyhedra would give Cu-Fe distances greater than 3.7 Å. That such distances in the Fourier

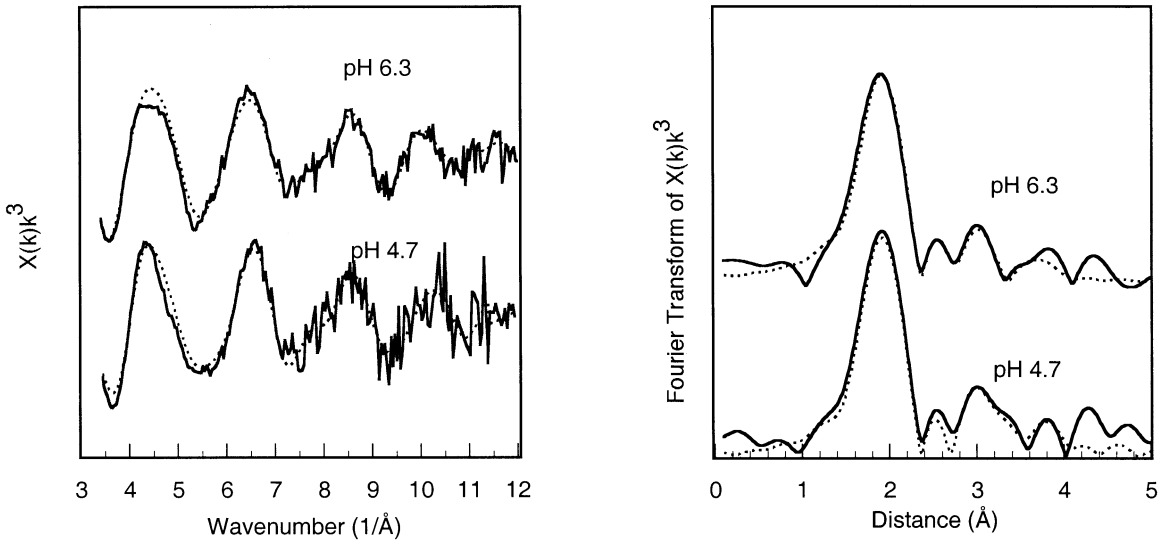

Fig. 7. EXAFS and Fourier transform of EXAFS for Cu(II) on goethite adsorption samples equilibrated with 25 ppm $[Cu]_{total}$.

transform can be modeled in terms of multiple scattering suggests that monodentate surface complexes are not important. However, we cannot completely rule out monodentate complexes.

To help verify the structural models for the surface complexes, we calculated the optimized geometries for clusters analogous to bidentate mononuclear corner-sharing and bidentate binuclear corner-sharing surface complexes (Figs. 10a and b, respectively) using density functional theory. The ab initio predicted bond lengths (Fig. 10) are in reasonable agreement with those observed via EXAFS for Cu adsorption on goethite, hematite and lepidocrocite (Table 1). Based on the effect of protonation on bond lengths, we propose the dimer to be protonated as $Cu_2O(OH)_5^{3-}$ (Fig. 10b).

Surface complexes analogous to those predicted with ab initio calculations are able to occur on the {100} and {101} faces of goethite (setting Pnma); the {110} and imperfect {001} faces of hematite (*R*-3c) and the {001} face of lepidocrocite (setting $Cmc2_1$). Note that we are using the standard space-group settings; our notation differs from that of other authors (e.g., Hiemstra and van Riemsdijk, 1996; Venema et al., 1998) for goethite and lepidocrocite.

With the results from our EXAFS spectroscopy we cannot rule out the possibility of bidentate edge-sharing between $(CuO_4H_n)^{n-6}$ and two oxygens on a single Fe site (e.g., at the {210} and {010} faces of goethite). An ab initio calculation, however, shows that a cluster analogous to the edge-sharing complex is somewhat less stable (15 kJ/mole) than the cluster analogous to the bidentate corner-sharing complex (Fig. 10a). Moreover, as is discussed below, the {210} and {010} faces in goethite comprise a very small fraction of the total surface area; the number of FeOH(H) sites due to these faces is not high enough to account for all the sorption displayed in our edges and isotherms. We show below that it is, in fact, unnecessary to include {210} and {010} edge-sharing FeOH(H) sites in the value for active surface site density as all the adsorption can be comfortably modeled with just corner-sharing FeOH(H) sites present on the {101} and {100} faces of goethite.

EXAFS data for synthetic $Cu(OH)_2$, shown in Figure 11 and summarized in Table 2, were fit according to the structural

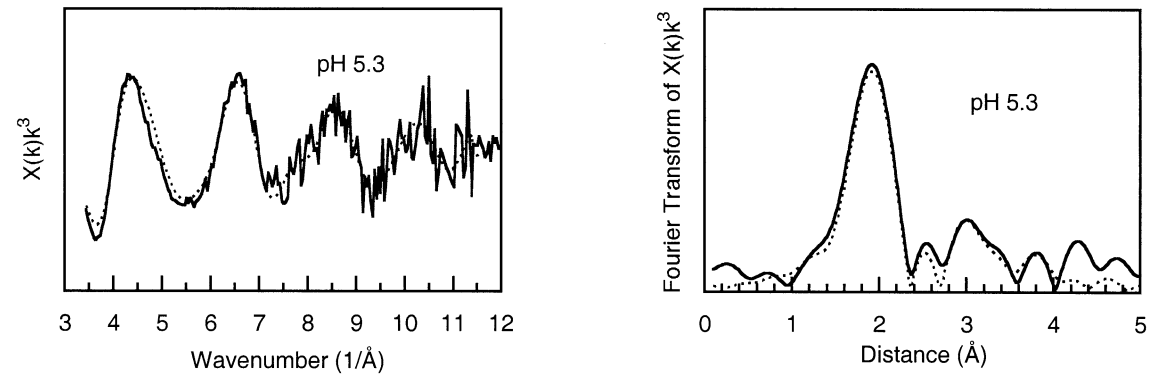

Fig. 8. EXAFS and Fourier transform of EXAFS for Cu(II) on hematite adsorption samples equilibrated with 25 ppm $[Cu]_{total}$.

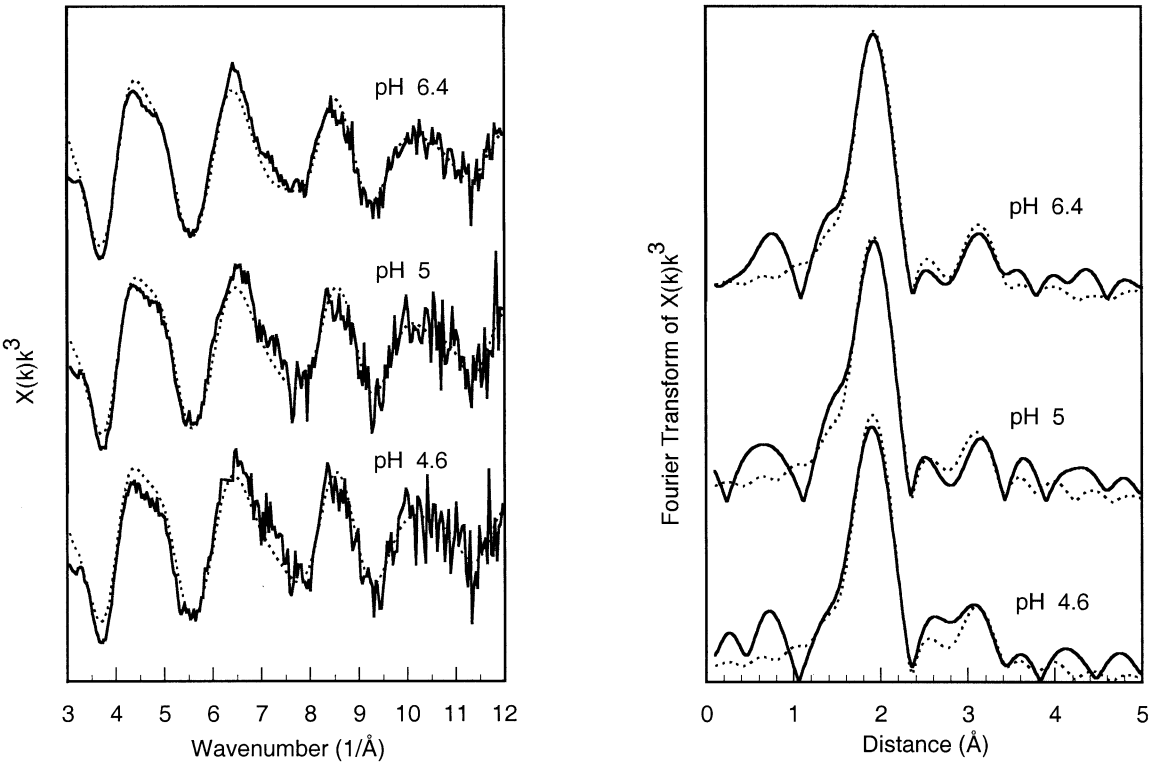

Fig. 9. EXAFS and Fourier transform of EXAFS for Cu(II) on lepidocrocite adsorption samples equilibrated with 25 ppm $[Cu]_{total}$.

model of Oswald et al. (1990). The local structural environment of Cu in $Cu(OH)_2$ is similar to that of Cu sorbed onto FeOOH/Fe_2O_3. However, we believe that the EXAFS confirm the absence of $Cu(OH)_2$ on the sorption samples: Using the same Debye-Waller factors as in $Cu(OH)_2$, we find only 1.0 (± 0.5) Cu neighbors at 2.9–3.0 Å and 2.0 (± 0.5) Fe at 3.2–3.4 Å in the Cu sorption samples. Note also that the EXAFS of the Cu-FeOOH samples at pH 6.3–6.4 are identical to those at pH

Table 1. Multiple scattering EXAFS fits for Cu(II) sorbed to goethite, hematite, and lepidocrocite.[a]

pH (wt %Cu)	N_O, R(Cu-O_1) ($2\sigma^2$)	N_O, R(Cu-O_2) ($2\sigma^2$)	N_O, R(Cu-O_3) ($2\sigma^2$)	N_O, R(Cu-O_4) ($2\sigma^2$)	N_O, R(Cu-O_5) ($2\sigma^2$)	N_{Cu}, R(Cu-Cu) ($2\sigma^2$)	N_{Fe}, R(Cu-Fe_1) ($2\sigma^2$)	N_{Fe}, R(Cu-Fe_2) ($2\sigma^2$)	X^2 (R %)
				Goethite					
4.7	*1.0*	*1.0*	*1.0*	*1.0*	*1.0*	0.9	1.3	1.2	2.52
(0.38)	1.86	1.98	2.00	2.11	2.29	2.97	3.14	3.33	(27.4)
	(0.001)	(0.005)	(0.001)	(0.007)	(0.013)	*(0.013)*	*(0.015)*	*(0.015)*	
6.3	*1.0*	*1.0*	*1.0*	*1.0*	*1.0*	1.0	1.6	1.2	2.23
(0.75)	1.87	1.98	2.00	2.09	2.29	2.99	3.21	3.41	(24.8)
	(0.002)	(0.005)	(0.002)	(0.005)	(0.013)	*(0.010)*	*(0.015)*	*(0.015)*	
				Hematite					
5.3	*1.0*	*1.0*	*1.0*	*1.0*	*1.0*	1.0	1.0	1.0	5.67
(0.73)	1.89	1.96	2.00	2.10	2.31	2.93	3.14	3.41	(35.7)
	(0.001)	(0.007)	(0.001)	(0.001)	(0.004)	*(0.010)*	*(0.015)*	*(0.015)*	
				Lepidocrocite					
4.6	*1.0*	*1.0*	*1.0*	*1.0*	*1.0*	1.0	1.0	1.0	5.14
(0.20)	1.86	1.95	1.99	2.06	2.29	3.02	3.09	3.24	(41.0)
	(0.003)	(0.002)	(0.002)	(0.009)	(0.010)	*(0.015)*	*(0.015)*	*(0.015)*	
5.0	*1.0*	*1.0*	1.0	*1.0*	*1.0*	1.0	1.0	1.0	4.31
(0.43)	1.84	1.95	1.98	2.05	2.28	3.01	3.09	3.25	(36.9)
	(0.003)	(0.001)	(0.001)	(0.012)	(0.015)	*(0.015)*	*(0.015)*	*(0.015)*	
6.4	*1.0*	*1.0*	*1.0*	*1.0*	*1.0*	1.0	1.0	1.0	2.41
(0.75)	1.86	1.94	2.01	2.02	2.26	3.07	3.03	3.24	(26.7)
	(0.007)	(0.001)	(0.01)	(0.001)	(0.019)	*(0.015)*	*(0.015)*	*(0.015)*	

[a] Values in italics were constrained during fitting. R is distance in Å; $2\sigma^2$ is Debye-Waller factor in $Å^2$; N_A is number of atoms of type A.

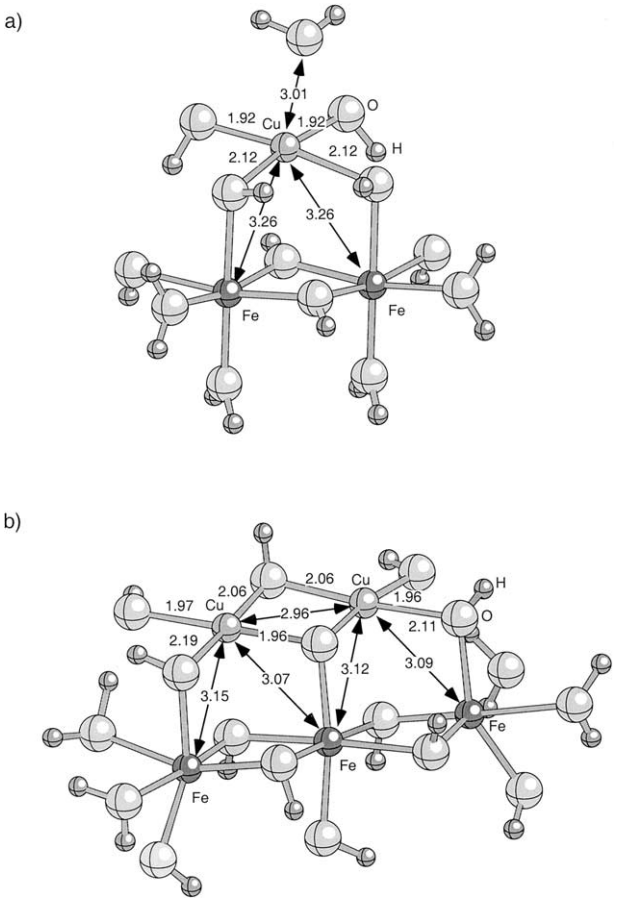

Fig. 10. Cu(II) ab initio molecular geometry clusters. (a) Bidentate corner-sharing mononuclear cluster. (b) Tridentate corner-sharing binuclear cluster. Bond lengths shown in Å. Both clusters give Cu-Fe and Cu-O bond lengths in good agreement with those observed in the EXAFS.

4.6–4.7 (where the system is unsaturated in $Cu(OH)_2$). Consequently, we argue that the EXAFS data indicate that $Cu(OH)_2$ has not precipitated on iron (hydr)oxide surfaces. Again, the absence of $Cu(OH)_2$ precipitation is indicated by the sorption isotherms at pH 6.5 discussed above. As will be shown below, the surface complexation model obtained by fitting the sorption edges is consistent with the complexes shown in Figure 10.

3.2. Surface Complexation Modeling

3.2.1. Equilibria at the Mineral Surface

The goethite, hematite and lepidocrocite mineral surfaces were modeled using the single-site 2-pK model, where the single surface adsorption site may exist in one of three protonation states; $\equiv SOH_2^+$, $\equiv SOH$ and $\equiv SO^-$. A homogeneous mineral surface with only one type of active surface functional group is assumed. Surface acidity constants are assigned to the reactions:

$$\equiv SOH + H^+ = \equiv SOH_2^+ \quad \log K_{a1} \tag{2}$$

$$\equiv SOH = \equiv SO^- + H^+ \quad \log K_{a2}, \tag{3}$$

where S is a nonspecific surface metal ion and $\equiv SOH_2^+$, $\equiv SOH$ and $\equiv SO^-$ are representative surface species.

The amphoteric treatment of a single surface site is generally recognized as a convenient modeling framework rather than a precise representation of actual functional groups existing at the mineral surface (Rustad et al., 1996). For iron oxyhydroxides in particular, a crystallographic consideration of the cleaved mineral surface (Hiemstra et al., 1989a,b) shows surface oxide ions to be coordinated by up to three metal ions. As such, reactions (2) and (3) underestimate somewhat the complexity of a mineral surface. However, there has been considerable success in modeling cation (and anion) sorption under this construct, especially when a single-site *multispecies* approach is applied (e.g., using the CCM: Palmqvist et al., 1997; using the DLM: Dzombak and Ali, 1996; using the TLM: Kosmulski, 1996). Recently, cation sorption data, previously modeled in a two-site or multisite approach, has been successfully remodeled in a single-site (multispecies) extended TLM framework (Criscenti and Sverjensky, 2002).

The DLM (Dzombak and Morel, 1990) and TLM (Hayes and Leckie, 1987; Hayes et al., 1988) were used to describe the electric double layer properties of the mineral surfaces. Mineral surface area was determined by BET analysis. Active surface site density was determined by a crystallographic consideration of the mineral surface and by fitting potentiometric titration data. Surface complexation involving ions of the background electrolyte was considered within the TLM framework, where NO_3^- and Na^+ were allowed to form outer sphere complexes at the β plane (Eqns. 4 and 5, Table 2).

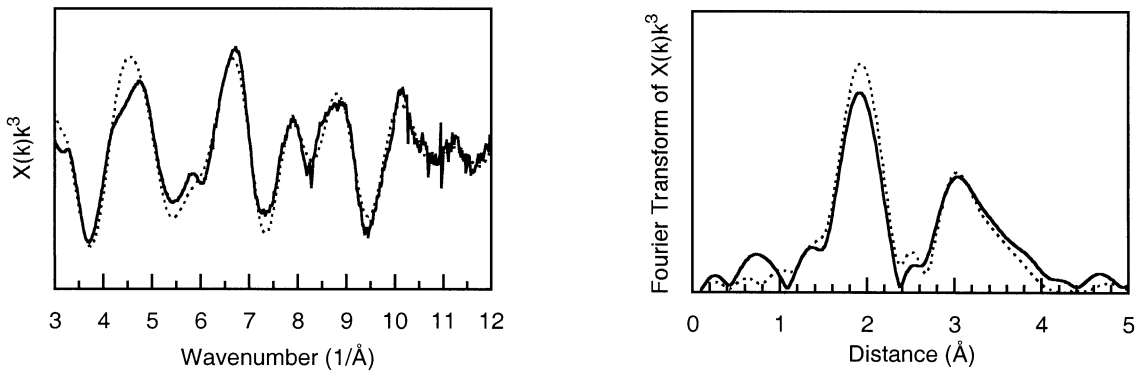

Fig. 11. EXAFS and Fourier transform of EXAFS for synthetic $Cu(OH)_2$.

Table 2. Multiple-scattering EXAFS parameters for $Cu(OH)_2$.[a]

N_O, R(Cu-O_1) ($2\sigma^2$)	N_O, R(Cu-O_2) ($2\sigma^2$)	N_O, R(Cu-O_3) ($2\sigma^2$)	N_O, R(Cu-O_4) ($2\sigma^2$)	N_{Cu}, R(Cu-Cu) ($2\sigma^2$)	N_{Cu}, R(Cu-Cu) ($2\sigma^2$)	N_{Fe}, R(Cu-Cu) ($2\sigma^2$)	N_{Fe}, R(Cu-Cu) ($2\sigma^2$)	X^2 (R %)
1.0	*1.0*	*1.0*	*1.0*	1.0	1.0	2.0	2.0	0.76
1.86	1.95	1.95	2.01	2.92	2.99	3.23	3.38	(32.0)
(0.001)	(0.009)	(0.006)	(0.005)	(0.015)	(*0.015*)	(*0.009*)	(*0.010*)	

[a] Values in italics were constrained during fitting. R is distance in Å; $2\sigma^2$ is Debye-Waller factor in $Å^2$; N_A is number of atoms of type A.

3.2.2. *Modeling Potentiometric Titration Data*

The DLM has three adjustable model parameters: a surface site density and two acidity constants. For hematite, we fixed the site density at the value (7.5 sites/nm^2) proposed by Venema et al. (1998). (This value is consistent with the site density estimated by modeling competitive sorption experiments for Cu and Pb on hematite; Christl and Kretzschmar, 1999.) For goethite, there are 3.03 FeO sites/nm^2 on {101} and 7.19 FeO sites/nm^2 on {100}. We arbitrarily fixed the site density at an average value of 6 sites/nm^2. Note that this is the same as that proposed by Hiemstra and van Riemsdijk (1996) for the total active surface site density. However, they arrived at this value by including the triply coordinated oxygens on {101} (which we assume are not involved in copper surface complexation) and neglecting the {100} surface. The values used for the surface site densities are consistent with what would be expected given the dominant crystal faces of the typical crystal morphologies. We then fit the potentiometric titration data to derive the surface acidity constants (Eqns. 2 and 3, Table 3). For lepidocrocite, we fit the total surface site density following the method of Hayes et al. (1991). The lepidocrocite sensitivity analysis yielded a unique set of parameter values for the surface acidity constants (Eqns. 2 and 3, Table 3) at the value of surface site density to produce the lowest goodness of fit parameter (V(Y)).

The TLM has six fitting parameters: site density, four equilibrium constants (two surface acidity constants and two electrolyte binding constants), and the capacitance of the inner Helmholtz plane, C_1. The capacitance of the outer Helmholtz plane (C_2) was assumed to be 0.2 F/m^2 following Hayes et al. (1991), Katz and Hayes (1995a,b) and Gao and Mucci (2001). Attempts to simultaneously fit all parameters did not converge; thus we adopted the modeling approach of Hayes et al. (1991). We determined a unique set of parameter values for goethite and hematite by fixing the site densities (as before) and the surface acidity constants (Eqn. 2 and 3, Table 3) and fitting for capacitance C_1 and electrolyte binding constants (Eqn. 4 and 5, Table 3). Surface acidity constants were then varied according to ΔpK_a ($-[(\text{Log } K^-) + (\text{Log } K^+)]$) to find the value of the electrolyte binding constants at the largest ΔpK_a to cause no change in the goodness of fit parameter (V(Y)). Hayes et al. (1991) include a detailed description of the procedure. Unique

Table 3. Mineral-Cu surface complexation model reactions.

Species	Mass action relation	Equilibrium constant
Mineral surface		
1) SOH	SOH	—
2) SOH_2^+	$SOH + H^+ = SOH_2^+$	K_{a1}
3) SO^-	$SOH = SO^- + H^+$	K_{a2}
4) $SO^- - Na^+$	$SOH + Na^+ = SO^- - Na^+ + H^+$	K_{cat}
5) $SOH_2^+ - NO_3^-$	$SOH + NO_3^- + H^+ = SOH_2^+ - NO_3^-$	K_{an}
Cu(II)		
Solution speciation		
6) $CuOH^+$	$Cu^{2+} + H_2O = CuOH^+ + H^+$	$K_{Hyd.1}$ ($10^{-8.2}$)[a]
7) $Cu_2(OH)_2^{2+}$	$2Cu^{2+} + 2H_2O = Cu_2(OH)_2^{2+} + 2H^+$	$K_{Hyd.2}$ ($10^{-10.59}$)[a]
8) $Cu(OH)_2$	$Cu^{2+} + 2H_2O = Cu(OH)_2 + 2H^+$	$K_{Hyd.3}$ ($10^{-17.5}$)[a]
9) H_2O	$H_2O = 2OH^- + H^+$	K_W ($10^{-13.79}$)[b]
Hypothetical surface complexes		
10) $SOCu^+$	$SOH + Cu^{2+} = SOCu^+ + H^+$	K_{10}
11) $SOHCu^{2+}$	$SOH + Cu^{2+} = SOHCu^{2+}$	K_{11}
12) $SOCuOH^0$	$SOH + Cu^{2+} + H_2O = SOCuOH^0 + 2H^+$	K_{12}
13) $SOHCuOH^+$	$SOH + Cu^{2+} + H_2O = SOHCuOH^+ + H^+$	K_{13}
14) $(SOH)_2Cu(OH)_2^0$	$2SOH + Cu^{2+} + 2H_2O = (SOH)_2Cu(OH)_2^0 + 2H^+$	K_{14}
15) $SOCu_2(OH)_2^+$	$SOH + 2Cu^{2+} + 2H_2O = SOCu_2(OH)_2 + 3H^+$	K_{15}
16) $S_2O_2Cu_2(OH)_2(OH)_2^0$	$2SOH + 2Cu^{2+} + 4H_2O = S_2O_2Cu_2(OH)_2(OH_2)_2^0 + 4H^+$	K_{16}
17) $(SOH)_2Cu_2(OH)_2(OH_2)_2^{2+}$	$2SOH + 2Cu^{2+} + 4H_2O = (SOH)_2Cu_2(OH)_2(OH_2)_2^{2+} + 2H^+$	K_{17}
18) $(S_3O(OH)_2)Cu_2(OH)_3^0$	$3SOH + 2Cu^{2+} + 3H_2O = (S_3O(OH)_2)Cu_2(OH)_3^0 + 4H^+$	K_{18}

[a] From Baes and Mesmer (1976).
[b] From Gunnarsson et al. (2000).

Table 4. Acid-base fits used in mineral-Cu surface complexation modeling.

	Goethite		Hematite		Lepidocrocite	
TLM	DLM	TLM	DLM	TLM	TLM	DLM
pH_{PZC}[a]	8.5	8.5	8.8	8.8	7.7	7.7
surface area(m^2/g)[b]	32.73	32.73	30.02	30.02	75.24	75.24
[SOH] (sites/nm^2)	6[c]	6[c]	7.5[c]	7.5[c]	1.6[d]	1.6[d]
log K_{a1}[d]	6.78	7.50	6.90	7.80	6.93	6.69
log K_{a2}[d]	−10.10	−9.50	−10.83	−9.80	−8.52	8.69
log K_{an}[d]		8.31		8.17		8.48
log K_{cat}[d]		−9.07		−10.02		7.18
C_1 (F/m^2)[d]		1.0		1.1		0.8
C_2 (F/m^2)[e]		0.2		0.2		0.2
V(Y)	85.0	9.8	71.0	8.0	31.2	4.7

[a] Determined from potentiometric titration data (this study).
[b] Determined from BET analysis (this study).
[c] Determined from a crystallographic consideration of the mineral surface (Hiemstra and van Riemsdijk, 1996; Venema et al., 1998).
[d] Determined from FITEQL simulation of potentiometric titration data (this study).
[e] From Katz and Hayes (1995a,b).

parameter values for lepidocrocite were determined by the same method but with an additional step at the beginning of the sensitivity analysis to find the optimal surface site density value. (Briefly, we fixed the surface acidity constants (Eqn. 2 and 3, Table 3) and fit for surface site density and electrolyte binding constants (Eqn. 4 and 5, Table 3). Surface site density was then fixed at the optimal value and the analysis method followed as for goethite and hematite. Hayes et al. (1991) include a detailed description of the procedure).

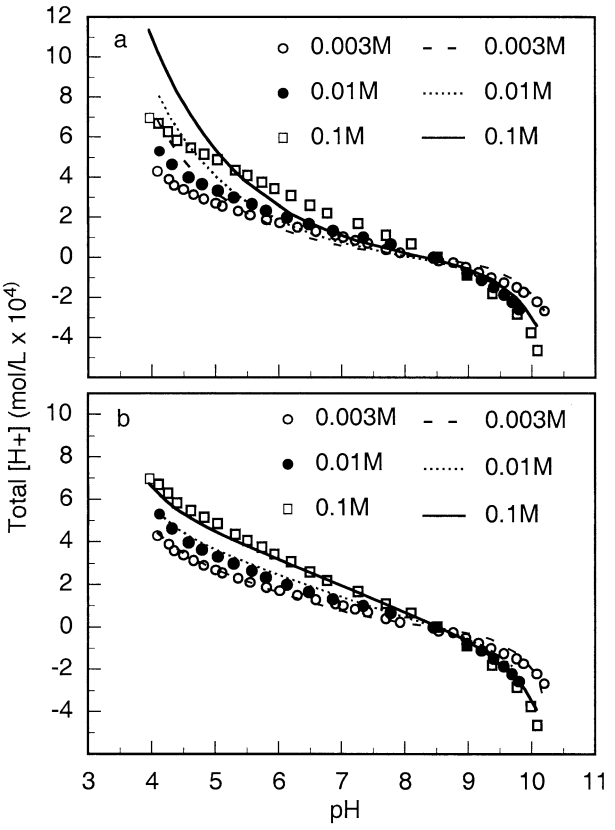

Fig. 12. Goethite potentiometric titration data at I = 0.003, 0.01 and 0.1 $NaNO_3$ and 25°C, shown as total [H^+] in mol/L; 6.63 g/L oxide. Symbols are data points; lines are model fits. (a) DLM. (b) TLM.

In passing, we find that fitting for goethite and hematite surface site density in both the DLM and TLM (following the method of Hayes et al., 1991) produces values similar (within 1.5 sites/nm^2) to those expected from crystallographic considerations. Our optimal value for lepidocrocite surface site density (Table 4) is also consistent with those previously reported (e.g., 1.67 sites/nm^2, Zhang et al., 1992).

Optimized acid-base parameter combinations are listed in Table 3 and the potentiometric titration data with model fits shown on Figures 12, 13 and 14. The experimental pH_{PZC} (the pH where the surface charge is zero) for goethite, hematite and lepidocrocite is the same (± 0.03 pH units for goethite, ± 0.01 pH units for hematite, ± 0.1 pH units for lepidocrocite) for all three ionic strengths measured. We report pH_{PZC} values of 8.5, 8.8 and 7.7 for goethite, hematite and lepidocrocite, respectively. These values lie within the range of reported experimental values (~7.5–9.5 for goethite and hematite and ~7–8 for lepidocrocite). Model fits of the acid-base data (Fig. 12, 13 and 14) show the TLM produces a very good replication of the data; the DLM fit is less satisfactory.

3.2.3. *Modeling Cu Adsorption Data*

The observed copper adsorption data was replicated in the DLM and TLM using the optimized acid-base parameter combinations (Table 4). Equilibria for reactions occurring in solution (Eqns. 6–8, Table 2) were taken from Baes and Mesmer (1976) which provides an internally consistent set of stability constants that includes the dimer complexes that form in solution.

3.2.4. *Cu^{2+} Complexation at the Surface of Goethite, Hematite, and Lepidocrocite*

A number of possible surface complexes (Eqns. 10–18, Table 3) were used in the attempt to model the observed copper adsorption. We include multinuclear surface complexation

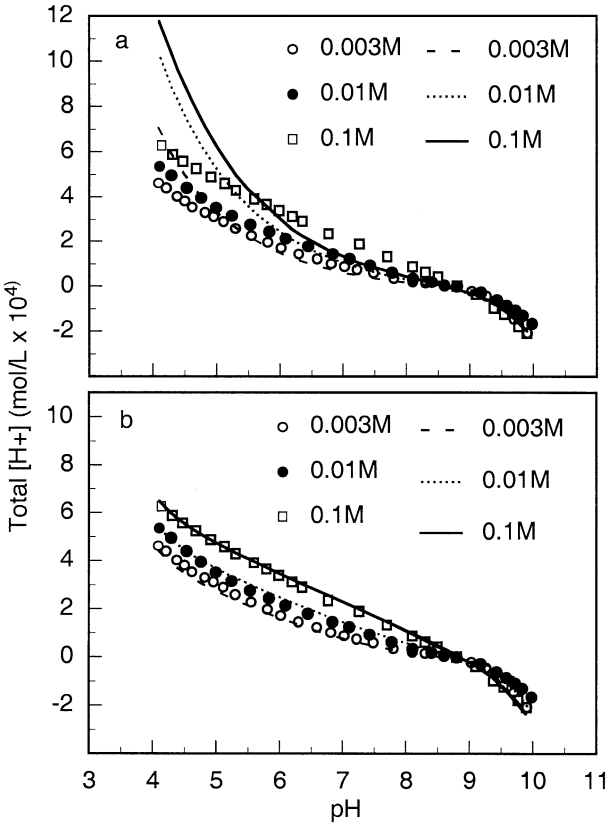

Fig. 13. Hematite potentiometric titration data at $I = 0.003$, 0.01 and 0.1 $NaNO_3$ and 25°C, shown as total $[H^+]$ in mol/L; 6.63 g/L oxide. Symbols are data points; lines are model fits. (a) DLM. (b) TLM.

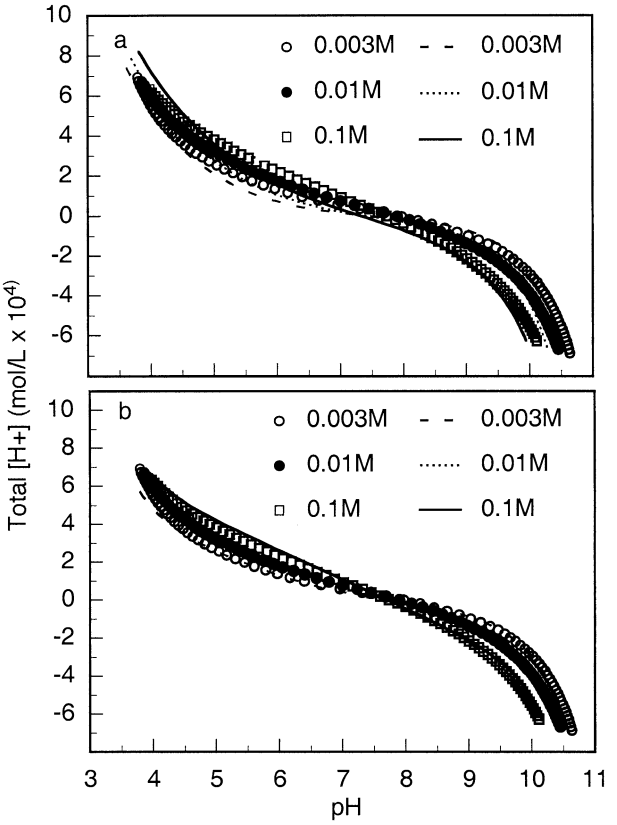

Fig. 14. Lepidocrocite potentiometric titration data at $I = 0.003$, 0.01 and 0.1 $NaNO_3$ and 25°C, shown as total $[H^+]$ in mol/L; 5 g/L oxide. Symbols are data points; lines are model fits. (a) DLM. (b) TLM.

(Eqns. 15–18, Table 3) in our modeling based on our direct spectroscopic evidence and ab initio predictions. This inclusion is in keeping with that of Katz and Hayes (1995a,b) who noted the need for multinuclear complexes to explain adsorption at moderate to high surface coverages. Furthermore, there is considerable additional spectroscopic evidence for the formation of surface polymers on oxide surfaces at moderate to high surface loadings (e.g., Cu(II), Bochatay et al., 1997; Cr(III), Eggleston and Stumm, 1993; Pb(II), Bargar et al., 1997).

The DLM fit to the copper(II) adsorption data is shown on Figures 3, 4 and 5 and summarized in Table 5. In both the DLM and TLM, surface species 10–18 were initially considered in a single species framework for adsorption on goethite, hematite and lepidocrocite between pH 2–7. In agreement with our EXAFS measurements and ab initio calculations, the formation of tridentate binuclear $(\equiv Fe_3O(OH)_2)Cu_2(OH)_3^0$ surface complexes (Eqn. 18, Table 3) provides the best fit to the observed copper adsorption data. We find binuclear surface complexes account for adsorption at moderate to high surface coverages in the higher pH range of the adsorption edges (in agreement with Katz and Hayes, 1995a,b). To improve the fit to the observed copper adsorption at low surface coverage (below pH ~4.5) on goethite, hematite and lepidocrocite, surface species 10–14 were considered in conjunction with binuclear surface complexes. We find this multispecies modeling approach provides the best fit to the adsorption data (in agreement with Criscenti and Sverjensky, 2002) by accounting for adsorption at both high and low surface coverage in the higher and lower pH range of the adsorption edges respectively. In light of our EXAFS measurements and ab initio predicted geometries, we fit the sorption edges using the tridentate binuclear $(\equiv Fe_3O(OH)_2)Cu_2(OH)_3^0$ complex

$$3{\equiv}FeOH + 2Cu^{2+} + 3H_2O = (\equiv Fe_3O(OH)_2)Cu_2(OH)_3^0 + 4H^+ \quad (4)$$

with stability constant

$$K((\equiv Fe_3O(OH)_2)Cu_2(OH)_3^0) = \frac{[(\equiv Fe_3O(OH)_2)Cu_2(OH)_3^0][H^+]^4}{[\equiv FeOH]^3[Cu^{2+}]^2} \quad (5)$$

and the bidentate mononuclear $(\equiv FeOH)_3Cu(OH)_2^0$ complex

$$2{\equiv}FeOH + Cu^{2+} + 2H_2O = (\equiv FeOH)_2Cu(OH)_2^0 + 2H^+ \quad (6)$$

with stability constant

$$K((\equiv FeOH)_2Cu(OH)_2^0) = \frac{[(\equiv FeOH)_2Cu(OH)_2^0][H^+]^2}{[\equiv FeOH]^2[Cu^{2+}]}, \quad (7)$$

where the surface species concentrations are given in moles/kg of water. Given the uncertainties in the coordination numbers (1.0 ± 0.5) due to copper neighbors at 2.9 Å, we cannot accurately resolve the relative fractions of monomer vs. dimer

Table 5. Predicted complexation of Cu^{2+} to goethite, hematite, and lepidocrocite.

Predicted metal complexes	Goethite		Hematite		Lepidocrocite	
	DLM	TLM	DLM	TLM	DLM	TLM
log K_{14}[a]	−3.10	−3.22	−3.60	−3.55	−2.40	−2.45
log K_{18}[a]	−5.25	−5.31	−5.90	−5.89	−4.23	−4.28
V(Y)	11.1	8.7	12.6	17.8	12.6	9.35

log K_{14}: log $K(SOH)_2Cu(OH)_2^0$: $2SOH + Cu^{2+} + 2H_2O = (SOH)_2Cu(OH)_2^0 + 2H^+$
log K_{18}: log $K(SOH)_2SOCu_2(OH)_3^0$: $3SOH + 2Cu^{2+} + 3H_2O = (SOH)_2SOCu_2(OH)_3^0 + 4H^+$

[a] From simulation of Cu sorption data (this study).

copper surface complexes using EXAFS spectroscopy. EXAFS shows that the dimer is present down to pH 4.6 and this is consistent with our surface complexation modeling of the sorption edges (Figs. 3, 4 and 5).

Both the DLM and the TLM successfully modeled the observed copper adsorption data. We find little change in equilibrium constants for predicted surface complexes and goodness of fit parameters when including outer sphere attraction of the background electrolyte ions (see Table 4). The fits shown (Figs. 3, 4 and 5) are therefore those generated in the simpler DLM modeling framework.

3.2.5. Activity Model for Surface Species

A better approach is to express the equilibrium constants in terms of activities of surface species. If we use a hypothetical standard state of complete coverage, then we can approximate the activity of a surface species as being the mole fraction of surface sites occupied by the species. In contrast, the molal standard state requires the stability constant of a multi-dentate surface complex to be a function of the concentration of the sorbent.

For the tridentate-dimer complex, at complete coverage (all surface sites used) we have

$$[(\equiv Fe_3O(OH)_2)Cu_2(OH)_3^0] = S_{tot}/2$$

so that

$$a_{(\equiv Fe_3O(OH)_2)Cu_2(OH)_3^0} = X_{(\equiv Fe_3O(OH)_2)Cu_2(OH)_3^0} = \frac{2[(\equiv Fe_3O(OH)_2)Cu_2(OH)_3^0]}{S_{tot}} \quad (8)$$

where S_{tot} is the total moles of surface sites/kg water. For the bidentate-mononuclear complex, we have, at complete coverage, $[(\equiv FeOH)_2Cu(OH)_2^0] = S_{tot}/2$ so that

$$a_{(\equiv FeOH)_2Cu(OH)_2^0} = X_{(\equiv FeOH)_2Cu(OH)_2^0} = \frac{2[(\equiv FeOH)_2Cu(OH)_2^0]}{S_{tot}}. \quad (9)$$

(In this scheme, we require, by definition, that bidentate-mononuclear complexes do not share surface hydroxyls with each other.) The activities of the ≡SOH sites will simply be their mole fractions: $X_{\equiv SOH} = [\equiv SOH]/S_{tot}$. The equilibrium constants then become

$$K((\equiv Fe_3O(OH)_2)Cu_2(OH)_3^0) = \left(\frac{S_{tot}^2}{2}\right)\frac{X_{((\equiv Fe_3O(OH)_2)Cu_2(OH)_3^0}[H^+]^4}{X_{\equiv FeOH}^3[Cu^{2+}]^2} \quad (10)$$

$$K((\equiv FeOH)_2Cu(OH)_2^0) = \left(\frac{S_{tot}}{2}\right)\frac{X_{(\equiv FeOH)_2Cu(OH)_2^0}[H^+]^2}{X_{\equiv FeOH}^2[Cu^{2+}]} \quad (11)$$

3.2.6. Test of Our Surface Complexation Model

We are able to fit our constant pH isotherm data (Fig. 6) to the surface complexation model proposed for the (pH edge) adsorption of copper to goethite, hematite and lepidocrocite. Using the log K constants derived in the pH edge data surface complexation modeling (Table 5) we fit our isotherm data in both the DLM and TLM. The DLM fits are shown on Figure 6 with V(Y) at 17.5 for goethite, 14.5 for hematite and 15.2 for lepidocrocite. Following Tamura and Furuichi (1997), theoretical surface density of adsorbed ions is the sum of the densities of the two types of surface complexes. The successful fitting of our isotherm data to the formation of tridentate binuclear $(\equiv Fe_3O(OH)_2)Cu_2(OH)_3^0$ complexes and bidentate mononuclear $(\equiv FeOH)_2Cu(OH)_2^0$ complexes is further evidence that precipitation of $Cu(OH)_2$ (s) and/or CuO (s) does not contribute to the apparent adsorption of Cu^{2+} to goethite, hematite and lepidocrocite.

To test our surface complexation model, we have fit our proposed surface complexes to previously published copper adsorption data on goethite (Ali and Dzombak, 1996) at an order of magnitude lower $[Cu]_{total}$ and an order of magnitude lower background electrolyte concentration ([BE]). We have modeled Cu^{2+} adsorption to goethite in the DLM at $[Cu]_{total} = 9.8 \times 10^{-5}$ M, [BE] = 0.1 mol/L (G1); $[Cu]_{total} = 9.8 \times 10^{-5}$ M, [BE] = 0.01 mol/L (G2); and $[Cu]_{total} = 2.3 \times 10^{-5}$ M, [BE] = 0.01 mol/L (G3). All surface complexation model parameters were as reported by Ali and Dzombak (1996; Table 6) except goethite surface site density which we fixed at our chosen value (6 sites/nm^2).

We are able to fit the data of Ali and Dzombak (1996) reasonably well to the formation of tridentate binuclear $(\equiv Fe_3O(OH)_2)Cu_2(OH)_3^0$ complexes and bidentate mononuclear $(\equiv FeOH)_2Cu(OH)_2^0$ complexes. The results of our modeling are shown in Figure 15 and summarized in Table 6. We find that the stability constants for the two surface complexes are similar (within 0.65) to those predicted for our own Cu^{2+} goethite adsorption data (at $[Cu]_{total} = 3.94 \times 10^{-4}$ M; [BE] =

Table 6. Predicted complexation of Cu^{2+} to goethite (data from Ali and Dzombak, 1996).

Surface complexation model parameters[a]			
pH_{PZC}			8.0 ± 0.1
Surface area (m^2/g)			79.4
log K_{a1}			7.68
log K_{a2}			−8.32
	Experimental conditions		
Metal complexes	G1	G2	G3
log K_{14}[b]	−3.65	−3.60	−3.25
log K_{18}[b]	−5.75	−5.90	−4.80
V(Y)	18.2	14.2	11.97

log K_{14}: log $K(SOH)_2Cu(OH)_2^0$: $2SOH + Cu^{2+} + 2H_2O = (SOH)_2Cu(OH)_2^0 + 2H^+$
log K_{18}: log $K(SOH)_2SOCu_2(OH)_3^0$: $3SOH + 2Cu^{2+} + 3H_2O = (SOH)_2SOCu_2(OH)_3^0 + 4H^+$
G1: $[Cu]_{total} = 9.8 \times 10^{-5}$ M, [BE] = 0.1 M
G2: $[Cu]_{total} = 9.8 \times 10^{-5}$ M, [BE] = 0.01 M
G3: $[Cu]_{total} = 2.3 \times 10^{-5}$ M, [BE] = 0.01 M

[a] As reported in Ali and Dzombak (1996).
[b] From simulation of Cu sorption data (data from Ali and Dzombak, 1996; simulation, this study).

0.1 mol/L $NaNO_3$). The low pH adsorption data (below pH 4.5) of Ali and Dzombak (1996) is fit less well by our surface complexation model than our own low pH Cu^{2+} adsorption data. However, in the pH region comparable to that investigated by EXAFS spectroscopy in this study (above pH 4.5), we model the formation of a dimer surface complex and this is consistent with our EXAFS results.

4. CONCLUSIONS

We measured the adsorption of Cu(II) onto goethite (α-FeOOH), hematite (α-Fe_2O_3) and lepidocrocite (γ-FeOOH) from pH 2–7. EXAFS spectra show that Cu(II) adsorbs as $(CuO_4H_n)^{n-6}$ and binuclear $(Cu_2O_6H_n)^{n-8}$ complexes. These form inner-sphere complexes with the iron (hydr)oxide surfaces by corner-sharing with two or three edge-sharing $Fe(O,OH)_6$ polyhedra. Our interpretation of the EXAFS data is supported by ab initio (density functional theory) geometries of analog $Fe_2(OH)_2(H_2O)_8Cu(OH)_4$ and $Fe_3(OH)_4(H_2O)_{10}Cu_2(OH)_6$ clusters. We find no evidence for surface complexes resulting from either monodentate corner-sharing or bidentate edge-sharing between $(CuO_4H_n)^{n-6}$ and $Fe(O,OH)_6$ polyhedra. Sorption isotherms and EXAFS spectra show that surface precipitates have not formed even though we are supersaturated with respect to CuO and $Cu(OH)_2$. Having identified the bidentate $(\equiv FeOH)_2Cu(OH)_2^0$ and tridentate $(\equiv Fe_3O(OH)_2)Cu_2(OH)_3^0$ surface complexes, we are able to fit the experimental copper(II) adsorption data to the reactions

$$3(\equiv FeOH) + 2Cu^{2+} + 3H_2O = (\equiv Fe_3O(OH)_2)Cu_2(OH)_3^0 + 4H^+$$

and

$$2(\equiv FeOH) + Cu^{2+} + 2H_2O = (\equiv FeOH)_2Cu(OH)_2^0 + 2H^+$$

The two stability constants are similar for the three iron (hydr)oxide phases investigated. In an encouraging test of our model we

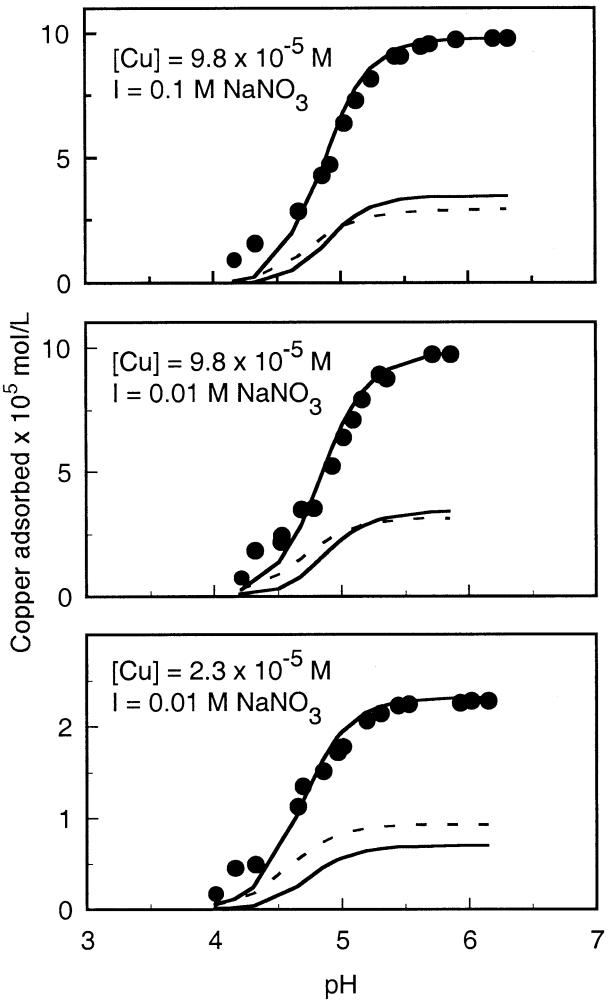

Fig. 15. Adsorption of copper(II) ions to goethite (α-FeOOH, 1.6 g/L) as a function of pH. Symbols are data points (from Ali and Dzombak, 1996); lines are DLM fits (this study) showing total and individual surface species (solid line = tridentate-dimer complex; dashed line = bidentate-mononuclear complex). Note that the concentration of copper due to the tridentate-dimer complex is twice that represented by the individual surface species solid line.

are also able to fit copper adsorption data at an order of magnitude lower $[Cu]_{total}$ and an order of magnitude lower background electrolyte concentration. Our surface complexation model disagrees with previous studies which invoked monodentate surface species (e.g., Ali and Dzombak, 1996; Robertson and Leckie, 1998). In those studies, monodentate complexes were able to provide a good fit to the sorption edges. This shows that it is difficult to unambiguously fit sorption edges to a surface complexation model without spectroscopic data.

Acknowledgments—Thanks are due to P. Chung Choi for assistance with ICP-AES analysis, Paul Moir-Riche and Chris Corrigan at Daresbury Materials Support Laboratory for XRD, and Bob Billsborrow at Daresbury Laboratory for support at Station 16.5. CLP was supported by a NERC studentship.

Associate editor: D. L. Sparks

REFERENCES

Ali M. A. and Dzombak D. A. (1996) Effects of simple organic acids on sorption of Cu^{2+} and Ca^{2+} on goethite. *Geochim. Cosmochim. Acta* **60,** 291–304.

Angove M. J., Wells J. D., and Johnson B. B. (1999) The influence of temperature on the adsorption of cadmium(II) and cobalt(II) on goethite. *J. Colloid Interface Sci.* **211,** 281–290.

Baes C. F. and Mesmer R. E. (1976) *The Hydrolysis of Cations*. Wiley.

Balistrieri L. S. and Murray J. W. (1982) The adsorption of Cu, Pb, Zn and Cd on goethite from major ion seawater. *Geochim. Cosmochim. Acta* **46,** 1253–1265.

Bargar J. R., Brown G. E., Jr., and Parks G. A. (1997) Surface complexation of Pb(II) at oxide-water interfaces: I. XAFS and bond-valence determination of mononuclear and polynuclear Pb(II) sorption products on aluminium oxides. *Geochim. Cosmochim. Acta* **61,** 2617–2637.

Binsted N. (1998) *Excurv98: The Manual*. Daresbury Laboratory, Warrington, UK.

Bochatay L., Persson P., Lovgren L., and Brown G. E., Jr.. (1997) XAFS study of Cu(II) at the water-goethite (α-FeOOH) interface. *J. Phy. IV* **7,** 819–820 (Colloque C2).

Bogdanov Y. A., Bortnikov N. S., Vikentev I. V., Gurvich E. G., and Sagalevich A. M. (1997) A new type of modern mineral-forming system: Black smokers of the hydrothermal field at 14 degrees 45′N latitude, Mid-Atlantic Ridge. *Geol. Ore Dep.* **39,** 58–78.

Bonnissel-Gissinger P., Alnot M., Ehrhardt J. J., and Behra P. (1998) Surface oxidation of pyrite as a function of pH. *Environ. Sci. Technol.* **32,** 2839–2845.

Boyle E. A., Sclater F. R., and Edmond J. M. (1977) The distribution of dissolved copper in the Pacific. *Earth Planet. Sci. Lett* **37,** 38–54.

Buerge-Weirich D., Hari R., Xue H., Behra P., and Sigg L. (2002) Adsorption of Cu, Cd, and Ni on goethite in the presence of natural groundwater Ligands. *Environ. Sci. Technol.* **36,** 328–336.

Callender E. and Bowser C. J. (1980) Manganese and copper geochemistry of interstitial fluids from manganese nodule-rich pelagic sediments of the northeastern equatorial pacific ocean. *Am. J. Sci.* **280,** 1063–1096.

Criscenti L. J. and Sverjensky D. A. (2002) A single-site model for divalent transition and heavy metal adsorption over a range of metal concentrations. *J. Colloid Interface Sci.* **253,** 329–352.

Christl I. and Kretzschmar R. (1999) Competitive sorption of copper and lead at the oxide-water interface: Implications for surface site density. *Geochim. Cosmochim. Acta* **63,** 2929–2938.

Christl I. and Kretzschmar R. (2001) Interaction of copper and fulvic acid at the hematite-water interface. *Geochim. Cosmochim. Acta* **65,** 3435–3442.

Davis J. A. (1982) Adsorption of natural dissolved organic matter at the oxide/water interface. *Geochim. Cosmochim. Acta* **46,** 2381–2393.

Dent A. J. and Mosselmans J. F. W. (1992) *A Guide to EXBACK, EXCALIB and EXCURV92*. CLRC Daresbury Laboratory, Warrington, UK.

Dzombak D. and Morel F. M. M. (1990) *Surface Complexation Modelling Hydrous Ferric Oxide*. Wiley.

Eggleston C. M. and Stumm W. (1993) Scanning-tunneling-microscopy of Cr(III) chemisorbed on α-Fe_2O_3 (001) surfaces from aqueous-solution—Direct observation of surface mobility and clustering. *Geochim. Cosmochim. Acta* **57,** 4843–4850.

Elderfield H. and Schultz A. (1996) Mid-ocean ridge hydrothermal fluxes and the chemical composition of the ocean. *Annu. Rev. Earth Planet Sci.* **24,** 191–224.

Farquhar M. L., Vaughan D. J., Hughes C. R., Charnock J. M., and England K. E. R. (1997) Experimental studies of the interaction of aqueous metal cations with mineral substrates: Lead, cadmium, and copper with perthitic feldspar, muscovite, and biotite. *Geochim. Cosmochim. Acta* **61,** 3051–3064.

Feely R. A., Massoth G. J., Baker E. T., Lebon G. T., and Geiselman T. L. (1992) Tracking the dispersal of hydrothermal plumes from the Juan de Fuca ridge using suspended mater composition. *J. Geophys. Res. Solid Earth* **97 (***B3***),** 3457–3468.

Fendorf S. E., LaForce M. J., Li G. C., and Patterson R. R. (1997) Pulsed-flow kinetic analysis of solid-phase transformations in mineral suspensions using XANES spectroscopy: Oxidation of FeS to γ-FeOOH (abstract). *Abstr. Am. Chem. Soc* **214,** 34-GEOC.

Fernex F., Fevrier G., Benaim J., and Arnoux A. (1992) Copper, lead and zinc trapping in Mediterranean deep-sea sediments: Probable coprecipitation with Mn and Fe. *Chem. Geol.* **98,** 293–306.

Gao Y. and Mucci A. (2001) Acid base reactions, phosphate and arsenate complexation, and their competitive adsorption at the surface of goethite in 0.7 M NaCl solution. *Geochim. Cosmochim. Acta.* **65,** 2361–2378.

Gans P. and O'Sullivan B. (2000) GLEE: A new computer program for glass electrode evaluation. *Talanta* **51,** 33–37.

Gunnarsson M., Jakobsson A., Ekberg S., Albinsson Y., and Ahlberg E. (2000) Sorption studies of cobalt(II) on colloidal hematite using potentiometry and radioactive tracer technique. *J. Colloid Interface Sci.* **231,** 326–336.

Hayes K. F. and Leckie J. O. (1987) Modelling ionic-strength effects on cation adsorption at hydrous oxide-solution interfaces. *J. Colloid Interface Sci.* **115,** 564–572.

Hayes K. F., Papelis C., and Leckie J. O. (1988) Modelling ionic-strength effects on anion adsorption at hydrous oxide-solution interfaces. *J. Colloid Interface Sci.* **125,** 717–726.

Hayes K. F., Redden G., Ela W., and Leckie J. O. (1991) Surface complexation models: An evaluation of model parameter estimation using FITEQL and oxide mineral titration data. *J. Colloid Interface Sci.* **142,** 448–469.

Hedin L. and Lundqvist S. (1969) Effects of electron-electron and electron-photon interactions on the one-electron states of solids. *Solid State Phys.* **23,** 1–181.

Herbelin A. and Westall J. (1996) *A Computer Program for Determination of Chemical Equilibrium Constants from Experimental Data*. Version 3.2. Department of Chemistry, Oregon State University, Corvallis, Oregon. 97331.

Herbert R. B. (1995) Precipitation of Fe oxyhydroxides and jarosite from acidic groundwater. *GFF* **117,** 81–85.

Hiemstra T., van Riemsdijk W. H., and Bolt H. (1989a) Multisite proton adsorption modeling at the solid/solution interface of (hydr) oxides: A new approach. Part I. *J. Colloid Interface Sci.* **133,** 91–104.

Hiemstra T., de Wit J. C. M., and van Riemsdijk W. H. (1989b) Multisite proton adsorption modeling at the solid/solution interface of (hydr) oxides: A new approach. Part II. *J. Colloid Interface Sci.* **133,** 105–117.

Hiemstra T. and Van Riemsdijk W. H. (1996) A surface structural approach to ion adsorption: The charge distribution (CD) model. *J. Colloid Interface Sci.* **179,** 488–508.

Ikhsan J., Johnson B., and Wells J. D. (1999) A comparative study of the adsorption of transition metals on kaolinite. *J. Colloid Interface Sci.* **217,** 403–410.

Juang R. and Wu W. (2002) Adsorption of sulphate and copper(II) on goethite in relation to the changes of zeta potentials. *J. Colloid Interface Sci.* **249,** 22–29.

Jung J., Cho Y., and Hahn P. (1998) Comparative study of Cu^{2+} adsorption on goethite, hematite and kaolinite: Mechanistic modelling approach. *Bull. Korean. Chem. Soc.* **19,** 324–327.

Katz L. E. and Hayes K. F. (1995a) Surface complexation modeling. I. Strategy for modeling monomer complex formation at moderate surface coverage. *J. Colloid Interface Sci.* **170,** 477–490.

Katz L. E. and Hayes K. F. (1995b) Surface complexation modeling. II. Strategy for modeling polymer and precipitation reactions at high surface coverage. *J. Colloid Interface Sci.* **170,** 491–501.

Karthikeyan K. G. and Elliott H. A. (1999) Surface complexation modeling of copper sorption by hydrous oxides of iron and aluminium. *J. Colloid Interface Sci.* **220,** 88–95.

Karthikeyan K. G., Elliott H. A., and Chorover J. (1999) Role of surface precipitation in copper sorption by the hydrous oxides of iron and aluminium. *J. Colloid Interface Sci.* **209,** 72–78.

Kosmulski M. (1996) Adsorption of cadmium on alumina and silica: Analysis of the values of stability constants of surface complexes calculated for different parameters of triple layer model. *Colloids Surf. A* **117,** 201–214.

Le Riche H. H. and Weir A. H. (1963) A method of studying trace elements in soil fractions. *J. Soil Sci.* **14,** 225–235.

Lovgren L., Sjoberg S., and Schindler P. W. (1990) Acid/base reactions and Al(III) complexation at the surface of goethite. *Geochim. Cosmochim. Acta* **54,** 1301–1306.

Lumsdon D. G. and Evans L. J. (1994) Surface complexation model parameters for goethite (α-FeOOH). *J. Colloid Interface Sci.* **164,** 119–125.

Nowack B., Lutzenkirchen J., Behra P., and Sigg L. (1996) Modeling the adsorption of metal-EDTA complexes onto oxides. *Environ. Sci. Technol.* **30,** 2397–2405.

Öhlander B., Thunberg J., Land M., Olof Höglund L., and Quishang H. (2003) Redistribution of trace metals in a mineralized spodosol due to weathering, Liikavaara, northern Sweden. *Appl. Geochem.* **18,** 883–899.

O'Melia C. R. (1989) Particle-particle interactions in aquatic systems. *Colloids Surf.* **39,** 255–271.

Oswald H. R., Reller A., Schmalle H., and Dubler E. (1990) Structure of copper(II) hydroxide, Cu $(OH)_2$. *Acta Crystall. C* **46,** 2279–2284.

Palmqvist U., Ahlberg E., Lövgren L., and Sjöberg S. (1997) In situ voltammetric determinations of metal ions in goethite suspensions: Single metal ion systems. *J. Colloid Interface Sci.* **196,** 254–266.

Parkman R. H., Charnock J. M., Bryan N. D., Livens F. R., and Vaughan D. J. (1999) Reactions of copper and cadmium ions in aqueous solution with goethite, lepidocrocite, mackinawite, and pyrite. *Am. Mineral.* **84,** 407–419.

Perdew J. P., Chevary J. A., Vosko S. H., Jackson K. A., Pederson M. R., Singh D. J., and Fiolhais C. (1992) Atoms, molecules, solids, and surfaces—Applications of the generalised gradient approximation for exchange and correlation. *Phy. Rev. B* **46,** 6671–6687.

Robertson A. P. and Leckie J. O. (1998) Acid/base, copper binding, and Cu^{2+}/H^+ exchange properties of goethite, an experimental and modelling study. *Environ. Sci. Technol.* **32,** 2519–2530.

Rodda D. P., Wells J. D., and Johnson B. B. (1996) Anomalous adsorption of copper(II) on goethite. *J. Colloid Interface Sci.* **184,** 564–569.

Rustad J. R., Felmy A. R., and Hay B. P. (1996) Molecular statics calculations of proton binding to goethite surfaces: A new approach to estimation of stability constants for multisite surface complexation models. *Geochim. Cosmochim. Acta* **60,** 1563–1576.

Savenko A. V. (2001) Coprecipitation of manganese, copper, zinc, lead, and cadmium with iron hydroxide in hydrothermal plumes—(By the data of laboratory modeling). *Oceanology* **41,** 502–507.

Schwertmann U. and Cornell R. M. (1991) *Iron Oxides in the Laboratory*. VCH Verlag.

Schwertmann U. and Fechter H. (1994) The formation of green rust and its transformation to lepidocrocite. *Clay Mineral.* **29,** 87–92.

Sherman D. M. (1985) Electronic structures of Fe^{3+} coordination sites in iron oxides: Applications to spectra, bonding and magnetism. *Phys. Chem. Mineral.* **12,** 161–175.

Tadanier C. J. and Eick M. J. (2002) Formulating the charge-distribution multisite surface complexation model using FITEQL. *Soil. Sci. Soc. Am. J.* **66,** 1505–1517.

Tamura H. and Furuichi R. (1997) Adsorption affinity of divalent heavy metal ions for metal oxides evaluated by modeling with the Frumkin isotherm. *J. Colloid Interface Sci.* **195,** 241–249.

te Velde G., Bickelhaupt F. M., Baerends E. J., Fonseca Guerra C., van Gisbergen S. J. A., Snijders J. G., and Ziegler T. (2001) Chemistry with ADF. *J. Computat. Chem.* **22,** 931–967.

Tessier A., Rapin F., and Carignan R. (1985) Trace-metals in oxic lake-sediments—Possible adsorption onto iron oxyhydroxide. *Geochim Cosmochim Acta* **49,** 183–194.

Vanos B., Visser H. J., Middelburg J. J., and Delange G. J. (1993) Occurrence of thin, metal-rich layers in deep-sea sediments—A geochemical characterization of copper remobilization. *Deep-Sea Res. 1* **40,** 1713–1730.

Venema P., Hiemstra T., Weidler P. G., and van Riemsdijk W. H. (1998) Intrinsic proton affinity of reactive surface groups of metal (hydr)oxides: Application to iron (hydr)oxides. *J. Colloid Interface Sci.* **198,** 282–295.

Vosko S. H., Wilk K., and Nusair M. (1980) Accurate spin-dependent electron liquid correlation energy for local spin density calculations: A critical analysis. *Can. J. Phys.* **1980,** 1200–1205.

Zhang Y., Charlet L., and Schindler P. W. (1992) Adsorption of protons, Fe(II) and Al(III) on lepidocrocite (gamma-FeOOH). *Colloids Surfaces* **63,** 259–268.